Induced-Fit in the Gas Phase: Conformational Effects on the Enantioselectivity of Chiral Tetra-Amide Macrocycles

ARTICLE *in* JOURNAL OF THE AMERICAN CHEMICAL SOCIETY · FEBRUARY 2008

Impact Factor: 12.11 · DOI: 10.1021/ja073287+ · Source: PubMed

J|A|C|S
ARTICLES
Published on Web 12/21/2007

Induced-Fit in the Gas Phase: Conformational Effects on the Enantioselectivity of Chiral Tetra-Amide Macrocycles

Francesco Gasparrini, Marco Pierini, Claudio Villani,* Antonello Filippi, and Maurizio Speranza*

Dipartimento degli Studi di Chimica e Tecnologia delle Sostanze Biologicamente Attive, Università La Sapienza, 00185 Roma, Italy

Received May 9, 2007; E-mail: maurizio.speranza@uniroma1.it

Abstract: The structure, stability, and reactivity of proton-bound diastereomeric $[M{\bullet}H{\bullet}A]^+$ complexes between some amino acid derivatives (A) and several chiral tetra-amide macrocycles (M) have been investigated in the gas phase by ESI-FT-ICR and ESI-ITMS-CID mass spectrometry. The displacement of the A guest from the diastereomeric $[M{\bullet}H{\bullet}A]^+$ complexes by reaction with the 2-aminobutane enantiomers (B) exhibits a distinct enantioselectivity with regards to the leaving amino acid A and, to a minor extent, to the amine reactant B. The emerging selectivity picture, discussed in the light of molecular mechanics calculations, provides compelling evidence that the most stable conformers of the selected chiral tetra-amide macrocycles M may acquire in the gas phase a different conformation by induced fit on complexation with some representative amino acid derivatives A. This leads to the coexistence in the gas phase of stable diastereomeric $[M{\bullet}H{\bullet}A]^+$ *eq*−*eq* and *ax*−*ax* structures, in proportions depending on the configuration of A and M and characterized by different stability and reactivity toward the 2-aminobutane enantiomers. The enantioselectivity of the gas-phase A-to-B displacement in the diastereomeric $[M{\bullet}H{\bullet}A]^+$ complexes essentially reflects the free energy gap between the homo- and heterochiral $[M{\bullet}H{\bullet}A]^+$ complexes, except when the tetra-amidic host presents an additional macrocycle generated by a decamethylene chain. In this case, the measured enantioselectivity mostly reflects the stability difference between the relevant diastereomeric transition structures.

Introduction

Shape-specific noncovalent attractive and repulsive interactions constitute the basis for information transfer between molecules in living systems as well as in synthetic supramolecular structures. Despite ever more accurate descriptions of biological systems and a dramatically increasing diversity of synthetic host/guest complexes, a systematic and general understanding of the underlying intermolecular forces is still in its infancy. Organic chemistry makes possible the targeted construction of infinitely variable macrocyclic compounds with multiple centers interacting in complementary ways.[1] Their remarkable selectivity toward a variety of neutral and ionic guests illustrates the principle of molecular recognition and is the basis of many applications.[2]

Perhaps the most widely known and extensively investigated macrocycles are crown ethers,[3] cryptands,[4] starands,[5] cyclodextrins,[6] and calixarenes.[7] Macrocyclic amides form another group of synthetic receptors that have been given considerable attention. Interest in this category of macrocyclic hosts comes from the amphiphilic properties of their amido groups in dipolar or H-bonding interactions, the carbonyl acting as a dipole donor and a H-bond acceptor and the N−H as a dipole acceptor and a H-bond donor. Indeed, a number of recent publications have presented convincing evidence that, depending on the experimental conditions, macrocyclic amides can bind cations or anions.[8] In general, it is thought that the complexation process will be energetically more favorable if the preferred conforma-

(1) (a) Lehn, J.-M. *Supramolecular Chemistry*; VCH: Weinheim, Germany, 1995. (b) Schneider, H.-J.; Yatsimirsky, A. *Principles and Methods in Supramolecular Chemistry*; Wiley: Chichester, U.K., 2000. (c) Steed, J. W.; Atwood, H. L. *Supramolecular Chemistry*; Wiley: Chichester, U.K., 2000. (d) Dietrich, B.; Viout, P.; Lehn, J.-M. *Macrocyclic Chemistry*; VCH: Weinheim, Germany, 1993.

(2) (a) Schneider, H. J. *Angew. Chem., Int. Ed. Engl.* **1991**, *30*, 1417. (b) Seel, C.; Vögtle, F. *Angew. Chem., Int. Ed. Engl.* **1992**, *31*, 528. (c) Izatt, R. M.; Pawlak, K.; Bradshow, J. S.; Bruening, R. L. *Chem. Rev.* **1991**, *91*, 1721.

(3) (a) Pedersen, C. J. *J. Am. Chem. Soc.* **1967**, *89*, 2495. (b) Pedersen, C. J. *Angew. Chem., Int. Ed. Engl.* **1988**, *27*, 1021. (c) Glendening, E. D.; Feller, D.; Thompson, M. A. *J. Am. Chem. Soc.* **1994**, *116*, 10657. (d) Glendening, E. D.; Feller, D. *J. Am. Chem. Soc.* **1996**, *118*, 6052.

(4) Lehn, J.-M. *Acc. Chem. Res.* **1978**, *11*, 49.

(5) (a) Cui, C.; Cho, S. J.; Kim, S. *J. Phys. Chem. A* **1998**, *102*, 1119. (b) Lee, W. Y.; Park, C. H.; Kim, S. *J. Am. Chem. Soc.* **1993**, *115*, 1184.

(6) Szejtli, J.; Osa, T. *Comprehensive Supramolecular Chemistry*; Cyclodextrines; Atwood, J. L., Davies, J. E. D., MacNicol, D. D., Vögtle, F., Eds.; Elsevier: Oxford, U.K., 1996; Vol. 3.

(7) (a) Mandolini, L.; Ungaro, R. *Calixarenes in Action*; Imperial College Press: London, U.K., 2000. (b) Perrin, M.; Oehler. In *Calixarenes, a Versatile Class of Macrocyclic Compounds*; Vicens, J., Böhmer, V., Eds.; Kluwer Academic Publishers: Dordrecht, The Netherlands, 1991.

(8) (a) Kim, H. Y.; Calabrese, J.; McEwen, C. *J. Am. Chem. Soc.* **1996**, *118*, 1545. (b) Kim, K. S.; Cui, C.; Cho, S. *J. Phys. Chem. B* **1998**, *102*, 461. (c) Malinowska, E.; Wróblewski, W.; Ostaszewski, R.; Jurczak, J. *Pol. J. Chem.* **2000**, *74*, 701. (d) Chmielewski, M.; Jurczak, J. *Tetrahedron Lett.* **2004**, *45*, 6007. (e) Szczepańska, A.; Sałański, P.; Jurczak, J. *Tetrahedron* **2003**, 4775. (f) Hossain, Md. A.; Llinares, J. M.; Powell, D.; Bowman-James, K. *Inorg. Chem.* **2001**, *40*, 2936. (g) Hossain, Md. A.; Kang, S. O.; Powell, D.; Bowman-James, K. *Inorg. Chem.* **2003**, *42*, 1397. (h) Suh, S. B.; Cui, C.; Son, H. S.; U., J. S.; Won, Y.; Kim, K. S. *J. Phys. Chem. B* **2002**, *106*, 2061. (i) Chmielewski, M.; Szumna, A.; Jurczak, J. *Tetrahedron Lett.* **2004**, *45*, 8699. (j) Chmielewski, M.; Jurczak, J. *Chem.*−*Eur. J.* **2005**, *11*, 6080.

10.1021/ja073287+ CCC: $40.75

Chart 1.[a]

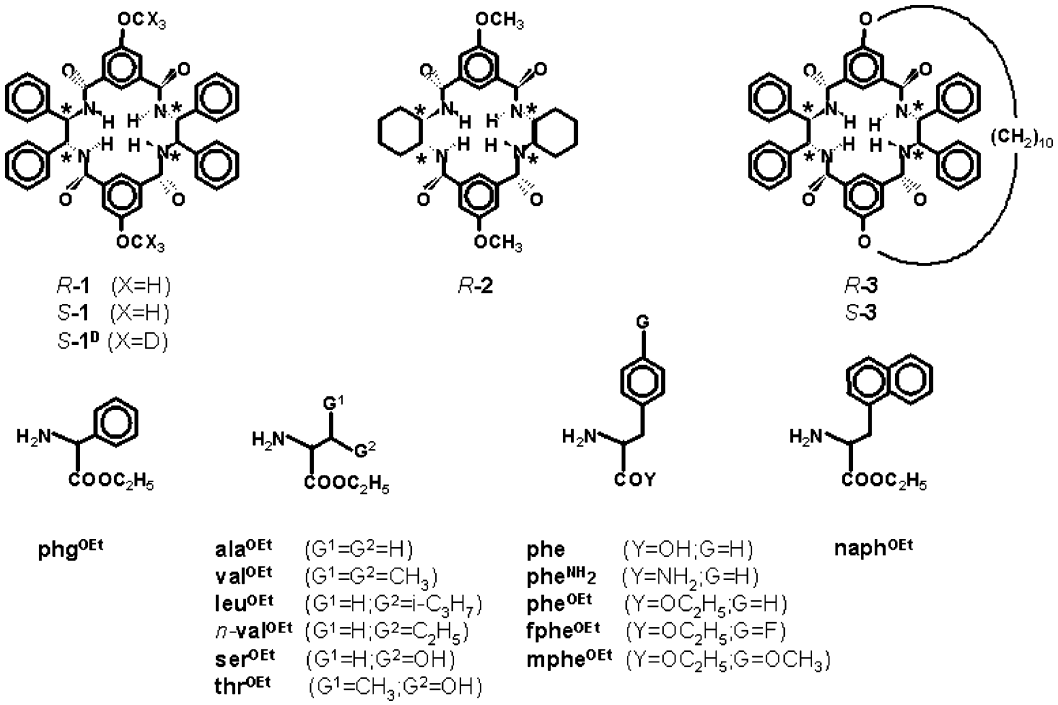

[a] *Configurational descriptors for chiral macrocycles **1**−**3** are abbreviated in the text as either *r* or *s*, meaning the configuration at the four stereogenic carbons are either *R,R,R,R* or *S,S,S,S*.

tion of the macrocycle in the free state resembles closely the conformation it will adopt upon interaction with the ionic guest. Thus, an important research endeavor is the study of the conformational equilibria of macrocyclic amide receptors and their sensitivity to the noncovalent interactions with potential guests.[9]

We were recently engaged in a preliminary mass spectrometric (MS) study of the chiral recognition of some representative amino acid derivatives (A), i.e., phenylalanine amide (**phe^{NH}2**), phenylalanine ethyl ester (**phe^{OEt}**), and naphthylalanine ethyl ester (**naph^{OEt}**) (Chart 1), by several specifically designed macrocyclic tetra-amides (M), i.e., *r*-**1**, *s*-**1**, and *r*-**2**, in the gas phase where interference from the solvent and the counterion is safely excluded.[10] The enantioselectivity of the selected M hosts was checked by introducing into a Fourier transform ion cyclotron resonance mass spectrometer (FT-ICR-MS), equipped with an electrospray ionization source (ESI), the proton-bonded two-body complexes $[M•H•A]^+$ and by measuring the rate of the displacement reaction 1 where B is either (*R*)-(−)- (B_R) and (*S*)-(+)-2-butylamine (B_S).

$$[M•H•A]^+ + B \rightarrow [M•H•B]^+ + A \qquad (1)$$

According to the relevant reaction kinetics, a single structure is attributed to the diastereomeric $[M•H•A]^+$ (M/A = *r*-**1**/**phe^{NH}2** and *r*-**2**/**phe^{OEt}**) complexes. In contrast, both the hetero-[*r*-**1**•H•*s*-**naph^{OEt}**]$^+$ and the homochiral [*s*-**1**•H•*s*-**naph^{OEt}**]$^+$ adducts behave as a combination of two stable, non-interconverting isomeric forms, one (henceforth marked with the *fast* subscript) much more reactive toward B than the other (henceforth marked with the *slow* subscript). Even more surprisingly is the observation of a single structure for the heterochiral [*r*-**1**•H•*s*-**phe^{OEt}**]$^+$ complex, whereas its homochiral [*r*-**1**•H• *r*-**phe^{OEt}**]$^+$ congener displays a reaction kinetics consistent with the coexistence of two stable [**1**•H•*r*-**phe^{OEt}**]$^+_{fast}$ and [**1**•H•*r*-**phe^{OEt}**]$^+_{slow}$ structures. No clear-cut explanation for such a spectacular configurational effect is presently available.

This intriguing kinetic picture prompted us to widen the investigation to the macrocyclic tetra-amides *s*-**1**^{D}, *r*-**3**, and *s*-**3** and to a larger set of amino acidic guests (Chart 1). The purposes of this research is to: (i) verify the effects of the functional groups of the guest A on the enantioselectivity of the gas-phase reaction 1; (ii) elucidate the structural features of the diastereomeric $[M•H•A]^+$ complexes; (iii) explain the origin of the spectacular configurational effect on the reactivity of isomeric forms of $[M•H•A]^+$ (A = **phe^{OEt}** and **naph^{OEt}**); and (iv) shed some light on the dynamics and the mechanism of reaction 1.

Results and Discussion

All of the experiments concerning the gas-phase thermodynamics and kinetics of the selected $[M•H•A]^+$ complexes have been carried out by using two complementary mass spectrometric techniques. Indications about the nature of proton bonding in the ESI-formed diastereomeric $[M•H•A]^+$ complexes have been derived from their collision-induced decomposition (CID) performed in a ion-trap mass spectrometer.[11−16] With the same instrument, information on the relative stability of diastereomeric

(9) Parra, R. D.; Yoo, B.; Welmhoff, M. *J. Phys. Chem. A* **2006**, *110*, 4487.
(10) Filippi, A.; Gasparrini, F.; Pierini, M.; Speranza, M.; Villani, C. *J. Am. Chem. Soc.* **2005**, *127*, 11912.
(11) Cooks, R. G.; Kruger, T. L. *J. Am. Chem. Soc.* **1977**, *99*, 1279.
(12) McLuckey, S. A.; Cameron, D.; Cooks, R. G. *J. Am. Chem. Soc.* **1981**, *103*, 1313.
(13) Cooks, R. G.; Patrick, J. S.; Kotiaho, T.; McLuckey, S. A. *Mass Spectrom. Rev.* **1994**, *13*, 287.
(14) Cooks, R. G.; Koskinen, J. T.; Thomas, P. D. *J. Mass Spectrom.* **1999**, *34*, 85.
(15) Armentrout, P. B. *J. Am. Soc. Mass Spectrom.* **2000**, *11*, 371.
(16) Dang, T. T.; Pedersen, S. F.; Leary, J. A. *J. Am. Soc. Mass Spectrom.* **1994**, *5*, 452.

Table 1. Enantioselectivity Factors *R* from CID of Diastereoisomeric $[(M)_2•H•A]^+$ Adducts

	Enantioselectivity Factor, *R*										
host (M)	Guest A										
	ala^{OEt}	val^{OEt}	leu^{OEt}	*n*-val^{OEt}	ser^{OEt}	thr^{OEt}	phg^{OEt}	phe^{OEt}	fphe^{OEt}	mphe^{OEt}	naph^{OEt}
r-**1**	1.93 ± 0.04	2.87 ± 0.03	3.13 ± 0.06	5.00 ± 0.01	3.00 ± 0.06	2.34 ± 0.05	2.35 ± 0.05	4.52 ± 0.09	3.07 ± 0.06	3.29 ± 0.07	10.00 ± 0.09
r-**2**	0.80 ± 0.02	1.18 ± 0.02	1.14 ± 0.02	1.10 ± 0.02	1.03 ± 0.02	1.19 ± 0.02	1.00 ± 0.02	1.81 ± 0.04	1.60 ± 0.03	1.48 ± 0.03	2.43 ± 0.05
r-**3**	1.37 ± 0.03	1.98 ± 0.04	1.61 ± 0.03	3.40 ± 0.07	1.19 ± 0.02	1.83 ± 0.04	1.56 ± 0.03	2.07 ± 0.04	2.22 ± 0.04	2.14 ± 0.04	1.51 ± 0.03

$[M•H•A]^+$ was obtained through CID of the corresponding $[M_2•H•A]^+$ aggregates.[17−19] The kinetic enantioselectivity of the exchange reaction 1 was determined by using an ESI-FT-ICR mass spectrometer. The enantioselectivity factors were obtained by comparing the rate constants of eq 1 when using the $[M•H•A]^+$ diastereoisomers with a given 2-butylamine (e.g., B_S) or, alternatively, by using a given $[M•H•A]^+$ diastereoisomer with the 2-butylamine enantiomers. In the next sections, these results will be summarized and integrated with those coming from dedicated molecular modeling and docking studies.

Gas-Phase Stability of Diastereomeric $[M•H•A]^+$ Complexes. Information about the relative stability of the homochiral and heterochiral $[M•H•A]^+$ complexes has been derived from CID of the corresponding three-body $[(M)_2•H•A]^+$ adducts. Their CID patterns are characterized by the exclusive formation of the relevant $[M•H•A]^+$ and $[(M)_2•H]^+$ fragments in proportions which depend on the relative basicity of the M/A and M/M adducts, the configuration of both the guest A and the host M, and the collision energies. At equal collision energies (see Experimental Section), the relative stability of the homochiral and heterochiral $[M•H•A]^+$ complexes from CID of the relevant $[(M)_2•H•A]^+$ adducts provides an expression of the enantioselectivity factor *R* of $[M•H]^+$ toward A (the subscripts *hetero*/*homo* refer to the relative configuration of the guest and the host in the complexes):[17−19]

$$R = \frac{\left(\frac{[M•H•A]^+}{[(M)_2•H]^+}\right)_{homo}}{\left(\frac{[M•H•A]^+}{[(M)_2•H]^+}\right)_{hetero}} \qquad (2)$$

Table 1 reports the enantioselectivity factors *R* for the $[M•H•A]^+$ complexes formed by combining all the *r*-M hosts and most of the A guests shown in Chart 1. Stereochemical preference is always in favor of the homochiral association ($R > 1$), with the only exception of **ala^{OEt}** with host **2**. The *R* values dramatically depend on the functional groups of both M and A. In general, they increase in the following M order: *r*-**2** < *r*-**3** < *r*-**1**, thus suggesting that the substituents bound to the stereogenic carbons of M play a major role. Another significant effect is attached to the decamethylene chain in **3**, which somewhat lowers its enantioselectivity relative to that of **1**. Comparison of the *R* factors of the complexes with A = **ala^{OEt}**, **val^{OEt}**, **leu^{OEt}**, and ***n*-val^{OEt}**, as guests, reveals an increase in enantioselectivity with the size of the aliphatic group of A. The presence of the OH functionality in A = **ser^{OEt}** and **thr^{OEt}** does not produce any effect on the selectivity. With aromatic A guests, the enantioselectivity factor *R*, measured with M = *r*-**1**, appears to strongly increase with the size of the π-systems (cfr. A = **phe^{OEt}** and A = **naph^{OEt}**) and with the chain flexibility (cfr. A = **phg^{OEt}** and A = **phe^{OEt}**). These factors play only a minor role with M = *r*-**2** and *r*-**3**. The presence of a *para*-substituent on the aromatic ring of A does not modify appreciably the enantioselectivity (cfr. A = **phe^{OEt}**, **fphe^{OEt}**, and **mphe^{OEt}**). The relative stability of diastereomeric $[M•H•A]^+$ complexes can be evaluated from the experimental *R* factors of Table 1 in terms of the following equation: $\Delta\Delta G_{CID} = (\Delta G_{hetero} - \Delta G_{homo})_{CID} = RT_{eff} \ln R$, at the "effective temperature" T_{eff}, which is an empirical parameter identified as the temperature of a canonical ensemble of clusters for which fragmentation would yield the same branching ratios as observed experimentally.[20]

Gas-Phase Reactivity of Diastereomeric $[M•H•A]^+$ Complexes. As pointed out above, the *R* factors of Table 1 reflect the relative stability of the heterochiral vs the homochiral $[M•H•A]^+$ fragments, and therefore, they express the thermodynamic enantioselectivity of the chiral $[M•H]^+$ hosts toward the chiral A guests, measured at the undefined "effective temperature" T_{eff}. Now, we are aimed at verifying whether the thermodynamic stability of $[M•H•A]^+$ is the only factor controlling its reactivity toward the amine B (eq 1). In other words, to what extent the relative stability of the diastereomeric $[M•H•A]^+$ complexes controls their enantioselectivity toward B.

Table 2 reports the ESI-FT-ICR kinetic parameters of the exchange reaction 1, measured in present and previous[10] studies. The kinetics were carried out by monitoring the appearance of the exchanged product $[M•H•B]^+$ and the decay of the reactant $[M•H•A]^+$ as a function of time *t*. If *I* is the intensity of complex $[M•H•A]^+$ at the delay time *t* and I_0 is the sum of the intensities of $[M•H•A]^+$ and $[M•H•B]^+$, monoexponential $\ln(I/I_0)$ vs *t* plots were obtained for all the systems with M = *r*-**1** and A = **phe** and **phe^{NH}2**, and with M = *r*-**2** and *A* = **phe**, **phe^{NH}2**, and **phe^{OEt}**. The good linearity of their decay curves (corr. coeff. $r^2 \geq 0.986$, see Supporting Information) confirms the view that the $[M•H•A]^+$ complexes are thermally equilibrated when reacting with B. The pseudo-first-order rate constants k' of reaction 1 were obtained from the slopes of the relevant $\ln(I/I_0)$ vs *t* linear plots. The corresponding second-order rate constants *k* are calculated from the ratio between the slope of the first-order plots and the B concentration ($k = k'/[B]$). Their values, compared with the relevant collision rate constants (k_C), estimated according to Su's trajectory calculation method,[21] provides directly the efficiency of the reaction (eff = k/k_C).

(17) For a recent review, see: Speranza, M. *Ad. Phys. Org. Chem.* **2004**, *39*, 147.
(18) Yao, Z.; Wan, T. S. M.; Kwong, K.; Che, C. *Chem. Commun.* **1999**, *20*, 2119.
(19) Tao, W. A.; Zhang, D.; Wang, F.; Thomas, P.; Cooks, R. G. *Anal. Chem.* **1999**, *71*, 4427.
(20) Laskin, J.; Futrell, J. H. *J. Phys. Chem.* **2000**, *104*, 8829.
(21) Su, T. *J. Chem. Phys.* **1988**, *88*, 4102, 5355.

Table 2. Exchange Rate Constants ($\times 10^{-11}$ cm^3 Molecule^{-1} s^{-1})

			B_R = (*R*)-(–)- $C_4H_9NH_2$		B_S = (*S*)-(+)- $C_4H_9NH_2$		
host (M)	guest (A)		k^a	ρ^b	k^a	ρ^b	ξ^b
r-**1**	*r*-**phe**		77.5 ± 1.0 (0.68)	0.86 ± 0.03	59.3 ± 0.6 (0.52)	0.96 ± 0.02	1.31 ± 0.03
r-**1**	*s*-**phe**		89.7 ± 1.5 (0.79)		61.9 ± 0.8 (0.55)		1.45 ± 0.04
r-**1**	*r*-**phe^{NH}2**		33.6 ± 0.7 (0.30)	0.83 ± 0.03	42.1 ± 0.5 (0.37)	0.87 ± 0.03	0.80 ± 0.02[c]
r-**1**	*s*-**phe^{NH}2**		40.4 ± 0.7 (0.36)		48.1 ± 1.1 (0.42)		0.84 ± 0.03[c]
r-**1**	*r*-**phe^{OEt}**	*fast*	26.3 ± 3.0 (0.24)	1.28 ± 0.18	25.2 ± 0.6 (0.22)	0.96 ± 0.02	1.04 ± 0.17
r-**1**	*s*-**phe^{OEt}**		20.6 ± 0.3 (0.18)		26.3 ± 0.3 (0.23)		0.78 ± 0.02
r-**1**	*r*-**phe^{OEt}**	*slow*	4.0 ± 0.2 (0.04)	0.19 ± 0.02	3.6 ± 0.2 (0.03)	0.14 ± 0.01	1.11 ± 0.12
r-**1**	*s*-**phe^{OEt}**		20.6 ± 0.3 (0.18)		26.3 ± 0.3 (0.23)		0.78 ± 0.02
s-**1^D**	*s*-**phe^{OEt}**	*fast*	26.2 ± 1.4 (0.23)	1.00 ± 0.08	23.0 ± 1.9 (0.20)	1.47 ± 0.35	0.88 ± 0.12[d]
s-**1^D**	*r*-**phe^{OEt}**		26.3 ± 0.7 (0.23)		15.6 ± 1.9(0.14)		0.59 ± 0.09[d]
s-**1^D**	*s*-**phe^{OEt}**	*slow*	4.44 ± 0.27 (0.039)	0.17 ± 0.01	2.77 ± 0.15 (0.024)	0.18 ± 0.03	0.62 ± 0.06[d]
s-**1^D**	*r*-**phe^{OEt}**		26.3 ± 0.7 (0.23)		15.6 ± 1.9(0.14)		0.59 ± 0.09[d]
s-**1**	*s*-**naph^{OEt}**	*fast*	1.22 ± 0.04 (0.010)	0.046 ± 0.004	1.25 ± 0.07 (0.011)	0.050 ± 0.009	0.98 ± 0.09[c]
r-**1**	*s*-**naph^{OEt}**	*fast*	26.3 ± 1.3 (0.22)		25.0 ± 2.5 (0.21)		1.05 ± 0.18[c]
s-**1**	*s*-**naph^{OEt}**	*slow*	0.064 ± 0.003 (0.0005)	0.052 ± 0.07	0.058 ± 0.007 (0.0005)	0.048 ± 0.09	1.10 ± 0.18[c]
r-**1**	*s*-**naph^{OEt}**	*slow*	1.23 ± 0.09 (0.010)		1.20 ± 0.06(0.010)		1.02 ± 0.04[c]
r-**2**	*r*-**phe**		89.6 ± 1.9(0.78)	1.39 ± 0.07	62.1 ± 2.4(0.54)	0.99 ± 0.05	1.44 ± 0.08
r-**2**	*s*-**phe**		64.6 ± 1.8(0.56)		62.9 ± 1.1 (0.55)		1.03 ± 0.03
r-**2**	*r*-**phe^{NH}2**		43.8 ± 1.4 (0.38)	1.05 ± 0.06	39.6 ± 0.5 (0.35)	0.93 ± 0.06	1.11 ± 0.07
r-**2**	*s*-**phe^{NH}2**		41.9 ± 1.3 (0.37)		42.5 ± 1.3 (0.37)		0.99 ± 0.06
r-**2**	*r*-**phe^{OEt}**		19.1 ± 0.2 (0.17)	0.65 ± 0.02	19.3 ± 0.6 (0.17)	0.62 ± 0.05	0.99 ± 0.04[c]
r-**2**	*s*-**phe^{OEt}**		29.2 ± 0.3 (0.26)		31.0 ± 1.2 (0.27)		0.94 ± 0.05[c]
s-**3**	*s*-**naph^{OEt}**	*fast*	23.9 ± 4.3 (0.19)	1.15 ± 0.28	24.9 ± 0.6(0.21)	0.72 ± 0.06	0.96 ± 0.05
r-**3**	*s*-**naph^{OEt}**	*fast*	20.8 ± 1.1 (0.18)		34.7 ± 2.0 (0.29)		0.60 ± 0.07
s-**3**	*s*-**naph^{OEt}**	*slow*	0.042 ± 0.003 (0.0004)	0.032 ± 0.005	0.051 ± 0.003 (0.0004)	0.044 ± 0.005	0.83 ± 0.14
r-**3**	*s*-**naph^{OEt}**	*slow*	1.32 ± 0.12 (0.012)		1.15 ± 0.09(0.010)		1.15 ± 0.19

[a] $k \times 10^{-11}$ cm^3 molecule^{-1} s^{-1}; the values in parentheses represent the reaction efficiency expressed as the ratio between the measured rate constants and the corresponding collision constant k_C, calculated using the trajectory calculation method (Su, T.; Chesnavitch, W. J. *J. Chem. Phys.* 1982, *76*, 5183). [b] $\rho = k_{homo}/k_{hetero}$ (referred to the configuration of M and A); $\xi = k_R/k_S$ (referred to the configuration of B). [c] Reference 10. [d] $\xi = k_S/k_R$ (referred to the configuration of B).

Like the above-mentioned systems, the heterochiral [*r*-**1**•H•*s*-**phe^{OEt}**]$^+$ complex follows a monoexponential kinetics when reacting with the B enantiomers (corr. coeff. $r^2 \geq 0.994$, see Supporting Information). Contrariwise, its homochiral [*r*-**1**•H•*r*-**phe^{OEt}**]$^+$ analogue follows a biexponential kinetics under the same experimental conditions. As pointed out in related studies,[10,22] this kinetic behavior conforms to the coexistence of two stable isomeric structures for [*r*-**1**•H•*r*-**phe^{OEt}**]$^+$, one less reactive ([*r*-**1**•H•*r*-**phe^{OEt}**]$^+_{slow}$) and the other more reactive ([*r*-**1**•H•*r*-**phe^{OEt}**]$^+_{fast}$). In contrast, the monoexponential kinetics, exhibited by the heterochiral [*r*-**1**•H•*s*-**phe^{OEt}**]$^+$ complex, is attributed to the occurrence of a single structure or, alternatively, of several stable isomers, but with comparable reactivity toward B. The same rationale applies to the monoexponential kinetics observed for the guest exchange reactions in the [*r*-**1**•H•*s*/*r*-**phe^{NH}2**]$^+$ and [*r*-**2**•H•A]$^+$ complexes.

We sought a definitive check of the spectacular configurational effect observed with [*r*-**1**•H•**phe^{OEt}**]$^+$ by replacing the *r*-**1** host with its hexadeuterated enantiomer *s*-**1^D**. The reaction kinetics of the corresponding [*s*-**1^D**•H•**phe^{OEt}**]$^+$ are extremely reassuring because, as expected, the heterochiral [*s*-**1^D**•H•*r*-**phe^{OEt}**]$^+$ complex displays a monoexponential kinetics, whereas the homochiral [*s*-**1^D**•H•*s*-**phe^{OEt}**]$^+$ one exhibits a biexponential decay plot. A different picture comes from the decay of the diastereomeric [**1**•H•*s*-**naph^{OEt}**]$^+$ and [**3**•H•*s*-**naph^{OEt}**]$^+$ complexes by reaction with the enantiomers of B. Both diastereomeric adducts show in fact biexponential decay curves, which suggest the presence of two persistent isomeric structures with largely different reactivity toward B (see Supporting Information).

An estimate of the relative abundance of the isomeric forms, responsible for the above biexponential kinetics, can be derived from the deconvolution of the corresponding $[MHA]^+$ decay curve. Accordingly, the time dependence of the more reactive isomer $[M•H•A]^+_{fast}$ can be inferred from the overall $[M•H•A]^+$ decay after subtracting the first-order decay of the less reactive isomer $[M•H•A]^+_{slow}$. The Y-intercepts of the first-order decay of $[MHA]^+_{slow}$ and $[MHA]^+_{fast}$ provide an estimate of the relative abundance of the $[MHA]^+$ isomers (Table 3). As expected, the same $[M•H•A]^+_{fast}/[M•H•A]^+_{slow} \approx 0.6$ distribution is observed for the homochiral [*r*-**1**•H•*r*-**phe^{OEt}**]$^+$ and [*s*-**1^D**•H•*s*-**phe^{OEt}**]$^+$complexes. With the diastereomeric [**1**•H•*s*-**naph^{OEt}**]$^+$ and [**3**•H•*s*-**naph^{OEt}**]$^+$ complexes, the $[M•H•A]^+_{fast}/[M•H•A]^+_{slow}$ distribution is more unbalanced in favor of the $[M•H•A]^+_{slow}$ component ($[M•H•A]^+_{fast}/[M•H•A]^+_{slow} \approx 0.1 \div 0.5$).

Kinetic Enantioselectivity. Table 2 reports the enantioselectivity of reaction 1 involving some representative $[M•H•A]^+$ complexes. The reaction enantioselectivity is expressed by the $\rho = k_{homo}/k_{hetero}$ ratio, when referred to the configuration of the A guest and the M host, or by the $\xi = k_R/k_S$ one, when referred to the configuration of the amine B. A $\rho > 1$ value indicates that the amine B displaces the guest from the homochiral complex faster that the guest from the heterochiral complex diastereomeric $[M•H•A_D]^+$ and $[M•H•A_L]^+$ complexes. The opposite is true when $\rho < 1$. A $\rho = 1$ value corresponds to equal displacement rates. Analogously, a $\xi > 1$ value indicates that the displacement of the A guest from a given $[M•H•A]^+$ diastereomer is faster with the *r*-amine (B_R) than with the *s*-one

(22) (a) Lebrilla, C. B. *Acc. Chem. Res.* **2001**, *34*, 653. (b) Wu, L.; Cooks, R. G. *Anal. Chem.* **2003**, *75*, 678. (c) Gal, J. F.; Stone, M.; Lebrilla, C. B. *Int. J. Mass Spectrom.* **2003**, *222*, 259. (d) Ahn, S.; Ramirez, J.; Grigorean, G.; Lebrilla, C. B. *J. Am. Soc. Mass Spectrom.* **2001**, *12*, 278. (e) Grigorean, G.; Lebrilla, C. B. *Anal. Chem.* **2001**, *73*, 1684.

Table 3. Percent Distribution of *eq*−*eq* and *ax*−*ax* Conformations for **phe^{NH2}**, **phe^{OEt}**, and **naph^{OEt}** Guests in $[M•H•A]^+$ Complexes

host (M)	guest (A)	$[M•H•A]^+$	$[M•H•A]^+_{fast}$ experimental	$[M•H•A]^+_{slow}$ experimental	$[M•H•A]^+_{fast}$ calculated (config.)	$[M•H•A]^+_{slow}$ calculated (config.)	$\Delta\Delta H°$(*fast-slow*)[a] (kcal mol^{-1})
1	**phe^{OEt}**	*homochiral*	37 ± 2	63 ± 2	17 (*ax*−*ax*)	83 (*eq*−*eq*)	0.9
		heterochiral	100		3 (*eq*−*eq*)	97 (*ax*−*ax*)	2.0
1^D	**phe^{OEt}**	*homochiral*	35 ± 8	65 ± 8	17 (*ax*−*ax*)	83 (*eq*−*eq*)	0.9
		heterochiral	100		3 (*eq*−*eq*)	97 (*ax*−*ax*)	2.0
1	**phe^{NH}2**	*homochiral*	100		27 (*ax*−*ax*)	73 (*eq*−*eq*)	0.6
		heterochiral	100		32 (*eq*−*eq*)	68 (*ax*−*ax*)	0.4
1	**naph^{OEt}**	*homochiral*	12 ± 3	88 ± 3	13 (*eq*−*eq*)	87 (*ax*−*ax*)	1.1
		heterochiral	29 ± 4	71 ± 4	21 (*eq*−*eq*)	79 (*ax*−*ax*)	0.8
2	**phe^{OEt}**	*homochiral*	100		100 (*eq*−*eq*)		
		heterochiral	100		100 (*eq*−*eq*)		
3	**naph^{OEt}**	*homochiral*	13 ± 2	87 ± 2	48 (*eq*−*eq*)	52 (*ax*−*ax*)	0.0
		heterochiral	34 ± 2	66 ± 2	8 (*eq*−*eq*)	92 (*ax*−*ax*)	1.5

[a] Derived from the MM calculated $[M•H•A]^+_{fast}$ and $[M•H•A]^+_{slow}$ relative abundances (columns 6 and 7); $\Delta\Delta H°(fast\text{-}slow) = \Delta H°_{fast} - \Delta H°_{slow} = -RT \ln([M•H•A]^+_{fast}/[M•H•A]^+_{slow})$, $T = 298$ K.

Table 4. Experimental and Calculated Enantioselectivities for Selected Host−Guest Combinations

$[M•H•A]^+$	$\Delta\Delta G^{\#}_{FT-ICR}$[a] (kcal mol^{-1})	$\Delta\Delta G_{CID}$[b] (kcal mol^{-1})	$\Delta\Delta G°_{th}$[c] (kcal mol^{-1})	$\Delta\Delta H°_{th}$[c] (kcal mol^{-1})
$[r\text{-}\mathbf{1}•H•\mathbf{phe}^{OEt}]^+$	1.05	0.89	0.91	0.83
$[r\text{-}\mathbf{1}•H•\mathbf{phe}^{NH2}]^+$	0.10	0.45	0.21	−0.25
$[r\text{-}\mathbf{1}•H•\mathbf{naph}^{OEt}]^+$	1.77	1.36	0.93	1.29
$[r\text{-}\mathbf{2}•H•\mathbf{phe}^{OEt}]^+$	0.27	0.35	0.54	0.09
$[r\text{-}\mathbf{3}•H•\mathbf{naph}^{OEt}]^+$	2.04	0.24	0.20	0.03
rmsd $_{FT-ICR/\,th}$[d]			0.92	0.95
rmsd $_{CID/\,th}$[d]			0.24	0.35

[a] $\Delta\Delta G^{\#}_{FT-ICR} = \Delta G^{\#}_{homo} - \Delta G^{\#}_{hetero} = -RT \ln \rho$ (Table 2), $T = 298$ K. [b] $\Delta\Delta G_{CID} = (\Delta G_{hetero} - \Delta G_{homo})_{CID} = RT_{eff} \ln R$ ($T_{eff} = 298$ K). [c] $\Delta\Delta X°_{th} = (\Delta X°_{hetero} - \Delta X°_{homo})_{th}$ ($X = G, H$), calculated at $T = 298$ K. [d] rmsd = root-mean-square deviation.

(B_S). Again, the opposite is true when $\xi < 1$. A $\xi = 1$ value corresponds to equal displacement rates.

From the measured kinetic enantioselectivity factors ρ of Table 2, it is possible to derive the $\Delta\Delta G^{\#}_{FT-ICR}$ difference between the activation barriers for the displacement reaction 1 involving the homochiral and the heterochiral $[M•H•A]^+$ clusters ($\Delta\Delta G^{\#}_{FT-ICR} = \Delta G^{\#}_{homo} - \Delta G^{\#}_{hetero} = -RT \ln \rho$). These quantities have been reported in Table 4 together with the $\Delta\Delta G_{CID} = (\Delta G_{hetero} - \Delta G_{homo})_{CID} = RT_{eff} \ln R$ values, calculated from the CID results of Table 1, by taking 298 K as the "effective temperature" T_{eff}.

The kinetic results of Table 2 confirm the view that the efficiency of the gas-phase reaction 1 may depend on the structure and the configuration of M, A, and B. The $[r\text{-}\mathbf{1}•H•A]^+$ (A = **phe** and **phe^{NH}2**) complexes exhibit a small enantioselectivity as regard to both the A ($0.8 < \rho < 1.0$) and the B configuration ($0.8 < \xi < 1.4$). Replacing *r*-**1** with *r*-**2** as host does not modify the picture appreciably ($0.9 < \rho < 1.4$ and $1.0 < \xi < 1.4$). In contrast, a more pronounced enantioselectivity, referred to the A configuration, is observed in the reaction with $[r\text{-}\mathbf{2}•H•\mathbf{phe}^{OEt}]^+$ ($\rho \approx 0.6$), whereas no effect of the B configuration is detected ($0.9 < \xi < 1.0$). As pointed out before, the decay curve of the heterochiral $[r\text{-}\mathbf{1}•H•s\text{-}\mathbf{phe}^{OEt}]^+$ complex reflects the occurrence of a single stable structure with a reaction efficiency of 0.18 (B_R) and 0.23 (B_S)). It is interesting to note that the reaction efficiency of the more reactive isomeric structure of the homochiral $[r\text{-}\mathbf{1}•H•r\text{-}\mathbf{phe}^{OEt}]^+$complex (eff = 0.24 ($B_R$); 0.22 ($B_S$)) is comparable to that of the single isomeric structure evidenced for the heterochiral $[r\text{-}\mathbf{1}•H•s\text{-}\mathbf{phe}^{OEt}]^+$ one.

The heterochiral $[s\text{-}\mathbf{1}^D•H•r\text{-}\mathbf{phe}^{OEt}]^+$ complex shows the same reaction efficiency (eff = 0.23 (B_R); 0.14 (B_S)) of its undeuterated $[r\text{-}\mathbf{1}•H•s\text{-}\mathbf{phe}^{OEt}]^+$ analogue (eff = 0.18 (B_R); 0.23 (B_S)). It should be considered that the efficiency of the reaction between heterochiral $[s\text{-}\mathbf{1}^D•H•r\text{-}\mathbf{phe}^{OEt}]^+$ complex and a given B enantiomer (eff = 0.23 (B_R); 0.14 (B_S)) must be compared with that between $[r\text{-}\mathbf{1}•H•s\text{-}\mathbf{phe}^{OEt}]^+$ and the opposite enantiomer of B (eff = 0.23 (B_S); 0.18 (B_R)). Similarly, the reaction efficiencies of the homochiral $[s\text{-}\mathbf{1}^D•H•s\text{-}\mathbf{phe}^{OEt}]^+_{fast}$ (eff = 0.23 (B_R); 0.20 (B_S)) and $[s\text{-}\mathbf{1}^D•H•s\text{-}\mathbf{phe}^{OEt}]^+_{slow}$ structure (eff = 0.04 (B_R); 0.02 (B_S)) closely correspond to those of their undeuterated $[r\text{-}\mathbf{1}•H•r\text{-}\mathbf{phe}^{OEt}]^+_{fast}$ and $[r\text{-}\mathbf{1}•H•r\text{-}\mathbf{phe}^{OEt}]^+_{slow}$ analogues (eff = 0.22 (B_S); 0.24 (B_R), and eff = 0.03 (B_S); 0.04 (B_R), respectively). The coincidence of these efficiency values, while reassuring about the accuracy and reproducibility of the experimental ESI-FT-ICR results, indicates no significant OCX_3 (X = H,D) kinetic isotope effects involved in their reaction 1.

Both the more and less reactive isomers of the diastereomeric $[\mathbf{1}•H•s\text{-}\mathbf{naph}^{OEt}]^+$ complexes display the same exceptional enantioselectivity, referred to the A configuration ($\rho = 0.050$), and a negligible selectivity toward the B enantiomers ($1.0 < \xi < 1.1$). A somewhat different picture is observed by replacing **1** with **3** as hosts. Here, the efficiency of reaction 1 involving the diastereomeric $[\mathbf{3}•H•s\text{-}\mathbf{naph}^{OEt}]^+_{fast}$ structures are almost identical to that measured for the heterochiral $[r\text{-}\mathbf{1}•H•s\text{-}\mathbf{naph}^{OEt}]^+_{fast}$ and $[s\text{-}\mathbf{1}^D•H•r\text{-}\mathbf{phe}^{OEt}]^+_{fast}$ ones (eff ≈ 0.2−0.3). The reaction enantioselectivity of the $[\mathbf{3}•H•s\text{-}\mathbf{naph}^{OEt}]^+_{fast}$ structures, relative to the A configuration ($0.72 < \rho < 1.15$), is significantly lower than that measured with the $[\mathbf{1}•H•s\text{-}\mathbf{naph}^{OEt}]^+_{fast}$ homologues ($\rho = 0.050$). A reversed order is observed for the less reactive $[M•H•s\text{-}\mathbf{naph}^{OEt}]^+_{slow}$ (M = **1**, **3**) structures. In fact, $0.032 < \rho < 0.044$ for $[\mathbf{3}•H•s\text{-}\mathbf{naph}^{OEt}]^+_{slow}$, whereas $\rho = 0.050$ for $[\mathbf{1}•H•s\text{-}\mathbf{naph}^{OEt}]^+_{slow}$. Similarly to $[\mathbf{1}•H•s\text{-}\mathbf{naph}^{OEt}]^+_{fast}$ and $[\mathbf{1}•H•s\text{-}\mathbf{naph}^{OEt}]^+_{slow}$, both $[\mathbf{3}•H•s\text{-}\mathbf{naph}^{OEt}]^+_{fast}$ and $[\mathbf{3}•H•s\text{-}\mathbf{naph}^{OEt}]^+_{slow}$ exhibit a limited selectivity toward the B enantiomers ($0.6 < \xi < 1.1$). The reduced enantioselectivity of the $[\mathbf{3}•H•s\text{-}\mathbf{naph}^{OEt}]^+_{fast}$ structures

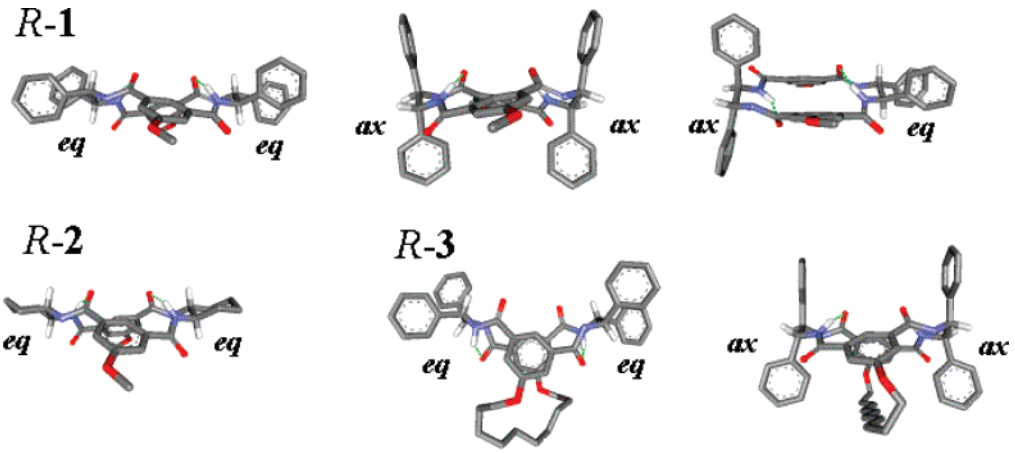

Figure 1. Relevant minimum energy structures of the *r*-**1**, *r*-**2**, and *r*-**3** hosts found by conformational search.

(ρ = 1.15 ± 0.28 (B_R); 0.72 ± 0.06 (B_S)) parallels the moderating effects of the decamethylene chain in **3** on the enantioselectivity factor *R* measured by ESI-MS−CID experiments. Furthermore, the presence of the hydrocarbon chain has no dramatic effects on the reaction efficiency, except for the [*s*-**1**•H•*s*-**naph**$^{\mathbf{OEt}}$]$^+_{fast}$ (eff = 0.01) and [*s*-**3**•H•*s*-**naph**$^{\mathbf{OEt}}$]$^+_{fast}$ (eff = 0.20) pair.

Molecular Modeling. Experimental results have clearly highlighted the ability of the tetra-amide macrocyclic hosts **1**−**3** to act as very effective selectors for the enantiomers of amino acid derivatives. Structural variations on both hosts and guests have sizable effects on enantioselectivity. To gain a better understanding of the factors determining the enantioselectivity of chiral hosts **1**−**3** toward the enantiomeric guests, we have performed an in-depth theoretical investigation based on molecular modeling calculations. Owing to the quite large size, flexibility, and complexity of the isolated hosts and their adducts, a reasonably complete and homogeneous sampling of the potential energy hypersurfaces related to the conformational variability of the single species and to the intermolecular host−guest interactions can only be obtained using computationally non-demanding methods. Our approach uses molecular mechanic models, that are computationally light and provide an excellent account of conformational energy differences for organic compounds. First, preliminary exhaustive conformational searches and relevant analyses have been carried out on structures of macrocycles M = *r*-**1,** *r*-**2,** and *r*-**3** and guests A = **phe**$^{\mathbf{OEt}}$, **phe**$^{\mathbf{NH}}$**2**, and **naph**$^{\mathbf{OEt}}$ by means of molecular mechanics using the MM2*force field (see Experimental Section). The more stable conformers of each species within a suitable energy window have been selected as the representative ensemble of their structure and employed to perform molecular docking simulations of [M•H•A]$^+$adducts, with guests in both *R* and *S* configuration (*r*-**1** with *r/s*-**phe**$^{\mathbf{OEt}}$, *r/s*-**phe**$^{\mathbf{NH}}$**2** and *r/s*-**naph**$^{\mathbf{OEt}}$; *r*-**2** with *r/s*-**phe**$^{\mathbf{OEt}}$; *r*-**3** with *r/s*-**naph**$^{\mathbf{OEt}}$). In turn, each type of proton-bound two-body complex is represented by an ensemble of adducts, again selected within an appropriately wide energy window, that describes geometry and stability of the complex as average properties. Standard structural enthalpy, entropy, and free energy changes ($\Delta X°_{hetero}$ and $\Delta X°_{homo}$, with X = *H*, *S*, or *G*) for each complexation process, and the corresponding differential terms between diastereomeric complexes ($\Delta\Delta X°_{th} = (\Delta X°_{hetero} - \Delta X°_{homo})_{th}$) have been derived by the statistical treatment of energetic data (eqs 3−5) and are collected in Table 4.

$$\Delta H°_{R/S} = \sum_{i=AD} H_i°_{R/S} \times p_i \quad (3)$$

$$\Delta S°_{R/S} = -\sum_{i=AD} p_i \times \ln(p_i) \quad (4)$$

$$\Delta G°_{R/S} = \Delta H°_{R/S} - T\Delta S°_{R/S} \quad (5)$$

(*AD* = number of adducts constituting the complex ensemble; p_i= Boltzmann population of the *i*° adduct inside the considered ensemble).

The geometry of the most stable proton-bound two-body complexes has been re-optimized at the B3LYP/6-31G* level of theory (see Supporting Information). Their inspection gave useful information as regards to the protonation site and the relative disposition/orientation of the components in each supramolecular adduct. In addition, the relative basicity of the host and the guest molecule within their supramolecular complexes were studied by quanto-mechanic calculations.

Calculated Structure and Energetics of the Tetramidic Hosts M. All the structures, obtained by the MM2* conformational searches of *r*-**1**, *r*-**2**, and *r*-**3** within an energy window of 4.5 kcal mol^{-1}, have been considered in the analysis. The calculated geometries of *r*-**1**, *r*-**2**, and *r*-**3** can be conveniently clustered in ensembles of three types, according to the dispositions assumed in each conformer by the alkyl or phenyl fragments on two contiguous stereogenic carbons of the host, denoted as C* in Chart 1. These geometries are classified as: equatorial−equatorial (*eq*−*eq*), axial−axial (*ax*−*ax*), and axial−equatorial (*ax*−*eq*) (Figure 1). Note that the cyclohexyl ring in *r*-**2** locks the position of the alkyl fragments on C* and only the *eq*−*eq* disposition is possible. In both *r*-**1** and *r*-**3**, the *eq*−*eq* dispositions are energetically favored, with Boltzmann populations (BP) amounting to 98.40% and 99.95%, respectively. In all *eq*−*eq* geometries, the macrocyclic host presents a *C*2-symmetric folded structure with a concave side and a convex one (Figure 2). Alternate and diverging CO and NH groups are located on the outer margins of the concave surface, F1, whereas the same, but now converging functionalities are placed on the central folding of the convex side, F2. Such molecular framework, reminding the structure of a saddle roof, is stabilized by two strong H-bonds between two facing amide moieties. For the three hosts, an additional distinction regards

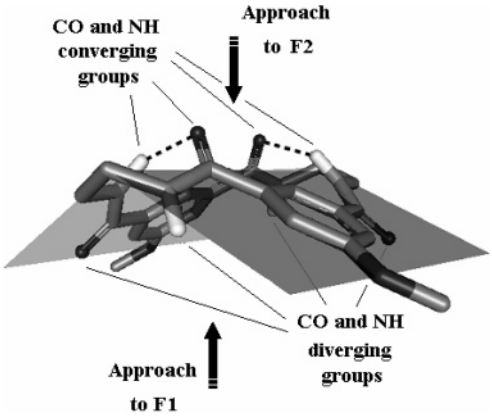

Figure 2. *C*2-symmetric saddle-roof structure of the selected *r*-**1**, *r*-**2**, and *r*-**3** hosts. Substituents on the stereogenic carbons are omitted for clarity.

the relevant *eq*−*eq* conformer ensembles. On the basis of the extent of their surface folding, it is possible to distinguish open and closed geometries (Figure 3) in which the angle formed by the two isophthalic rings is either larger or smaller than 100°, respectively. In the open structures, H-bonds are seen between C═O and N−H groups located on the F2 side, whereas in the closed structures these interactions are located on the F1 side.

In both *r*-**1** and *r*-**2**, the open *eq*−*eq* conformation results strongly favored over the closed one, while the reverse is true in **3**. This is certainly due to the decamethylene chain that connects the isophthalic rings and forces them in a nearly parallel disposition (Figure 1). Instead, within the less populated *ax*−*eq* and *ax*−*ax* geometries of *r*-**1** (1.6% of BP) and *r*-**3** (∼0.1% of BP) and also in the quasi-planar geometries of **2** (of negligible BP; Figure 1), the two isophthalic rings assume a wide-open disposition with the angle between the rings close to 150° in *ax*−*ax* conformers, and practically 180° in the other cases (Figure 3). Also in these structures, however, the four amidic fragments are complementarily arranged and establish a couple of intramolecular H-bonds. Inspection of both *r*-**1** and *r*-**2** molecular models clearly suggests that, in their *eq*−*eq* and *ax*−*ax* geometries, the F1 and F2 surfaces may easily interchange by inversion of the macrocycle through rotation around the aryl-CO bonds.

Docking experiments were then performed on highly representative conformers of the hosts molecules: six for *r*-**1** (three *eq*−*eq*, two *ax*−*ax* and one *ax*−*eq*), two for *r*-**2** (open *eq*−*eq* and closed *eq*−*eq*) and three for *r*-**3** (open *eq*−*eq* and closed *eq*−*eq* and one *ax*−*ax*).

Calculated Structure and Energetics of the Guest Molecules A. Molecular structures of the guests **phe**$^{\mathbf{OEt}}$, **phe**$^{\mathbf{NH}}$**2**, and **naph**$^{\mathbf{OEt}}$ have been modeled by starting the conformational search from their protonated forms at the amino groups. During the docking simulation, the protonated amino group of each guest acts as a probe for the basic sites present in the macrocyclic host. Conformers of each guest species for the docking experiments were selected within a 3 kcal mol^{-1} energy window among the large ensembles obtained by the conformational searches. To adequately simulate the high flexibility of the guests, such minimal ensembles were built according to the geometric criterion to warrant an exhaustive sampling of the wider dihedral angles diversity of all the rotatable bonds. The number of geometries considered in each cluster were 9 for **phe**$^{\mathbf{OEt}}$ (corresponding to 100% of BP), 5 for **phe**$^{\mathbf{NH}}$**2** (corresponding to 100% of BP) and 6 for **naph**$^{\mathbf{OEt}}$ (corresponding to 71% of BP).

Relative Basicity of the Host and the Guest in the [M•H•A]$^+$ Complexes. In all the [M•H•A]$^+$ systems investigated, [M•H]$^+$ is invariably the predominant, if not the exclusive CID fragment observed. These findings indicate that all the selected macrocyclic tetramides **1**−**3** of Chart 1 are significantly more basic than all the listed A guests. However, this basicity order is valid for M and A *in their isolated gaseous state*, whereas no indication about the proton location in the [M•H•A]$^+$ complexes may be derived by the experimental data. Protonation sites in the [M•H•A]$^+$ complexes have been therefore investigated by considering the adduct structures coming from the docking simulations both as such and after their further optimization by ab initio DFT-calculations, at the B3LYP/6-31G* level of theory (some of them have been re-optimized at the B3LYP/6-311+G** level of theory without any appreciable structural differences). In particular, optimizations were carried out: (i) directly on the more stable simulated complexes [*r*-**1**•H•*r*-**phe**$^{\mathbf{OEt}}$]$^+$ and [*r*-**1**•H•*s*-**phe**$^{\mathbf{OEt}}$]$^+$ having the host with different conformations (*eq*−*eq*, *ax*−*ax*, and *ax*−*eq*) and in which H$^+$ is bound to the amino group of the guest; (ii) on the same complexes previously modified by transferring the H$^+$ from the protonated amino group of the guest to the opposite

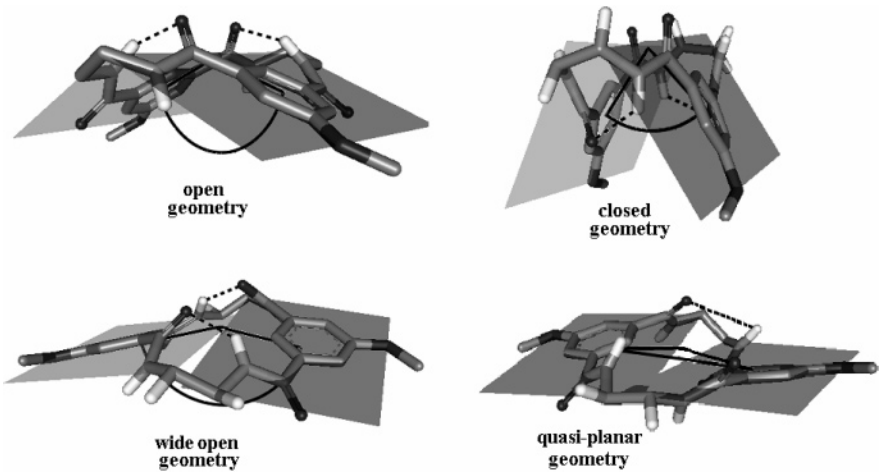

Figure 3. Models of the *r*-**1**, *r*-**2**, and *r*-**3** macrocycles showing their different folding patterns. Substituents on the stereogenic carbons are omitted for clarity.

carbonyl oxygen of the host. All the B3LYP/6-31G*-optimized structures are reported as Supporting Information (Figure S1). Inspection of these structures reveals that, irrespective of the input protonation site of the complex (whether on the most basic CO groups[23] of M or on the amino group of A), after DFT optimization the proton is invariably found on the amino group of A. This suggests that the **phe^{OEt}** molecule, which is less basic than M in the isolated state, *becomes more basic than M when "solvated" by the polar environment of the host*. The energetic cost for the proton transfer from M to the amino group of A in $[M•H•A]^+$ is largely counterbalanced by the extra-stabilization of the protonated A due to the establishment of multiple H^+-bondings between its NH_3^+ group and the amido carbonyls of M. Obviously, when these H^+-interactions are weakened in the CID excited $[M•H•A]^+$, such an extra-stabilization is largely removed and the proton moves to M because of the reduced basicity of the A guest.

Structure and Energetics of the $[M•H•A]^+$ Complexes. Supramolecular generation of some of the $[M•H•A]^+$ adducts studied in the present work was simulated by multiconformational molecular docking procedures, characterized by high-grid sampling levels of both the host approaching surface and the guest geometrical orientation.[24] We modeled the following diastereomeric pairs of complexes: [*r*-**1**•H•*s*/*r*-**phe^{OEt}**]$^+$, [*r*-**1**•H•*s*/*r*-**phe^{NH}2**]$^+$, [*r*-**1**•H•*s*/*r*-**naph^{OEt}**]$^+$, [*r*-**2**•H•*s*/*r*-**phe^{OEt}**]$^+$, and [*r*-**3**•H•*s*/*r*-**naph^{OEt}**]$^+$, with a number of adducts of each species generated in the first step of the docking procedure equal to 763 776, 424 320, 509 184, 254 592, and 254 592, respectively. Inspection of the more stable complexes shows that, irrespective of the type and configuration of host and guest species, a pattern of strong H-bonds is established between the two molecular units at the center of the macrocycle convex side. In particular, the protonated amino group of the guest is always H^+-bonded to the converging C═O groups present on the F2 surface. By contrast, all the adducts formed with the guest approaching the host from the concave surface are computed about 17 kcal mol^{-1} higher in energy. Interestingly enough, only the *eq*−*eq* and *ax*−*ax* conformations of the macrocycles are found in the ensembles of the more stable adducts and *in proportions different from those of the uncomplexed hosts*. In particular, host *r*-**1,** that in the free form is calculated to assume almost exclusively the *eq*−*eq* conformation ([*eq*−*eq* BP] > 98%), acquires a predominant *ax*−*ax* geometry by induced fit on complexation with *s*-**phe^{OEt}**, *s*-**phe^{NH}2**, and *r*/*s*-**naph^{OEt}** guests (68%< [*ax*−*ax* BP] <97%; Table 3). Among the minority *eq*−*eq* conformations, the more stable ones show open geometries. Similarly, host *r*-**3,** that is almost exclusively *eq*−*eq* in the free state (*eq*−*eq* BP ≈ 100%), is calculated to assume a predominant *ax*−*ax* geometry by induced fit on complexation with *s*-**naph^{OEt}** ([*eq*−*eq* BP] ≈ 8%) and, to a lesser extent, on complexation with the *r*-**naph^{OEt}** ([*eq*−*eq* BP] ≈ 48%). Even in this case, the more stable among the minority *eq*−*eq* conformations adopt only open geometries. In contrast, host *r*-**2** undergoes only a population change of its own *eq*−*eq* geometry by induced fit on complexation with the *r*/*s*-**phe^{OEt}** guest enantiomers: after addition of the guest, a significant fraction of the adducts generated starting with the host in the minority closed conformation shows this latter in the open form.

For the homochiral [*r*-**1**•H•*r*-**phe^{OEt}**]$^+$ and [*s*-**1^D**•H•*s*-**phe^{OEt}**]$^+$-complexes, MM calculations point to their *eq*−*eq* structures as 0.9 kcal mol^{-1} more stable than the corresponding *ax*−*ax* ones ($\Delta\Delta H°_{(fast-slow)}$ in Table 3). The order is reversed in the heterochiral [*r*-**1**•H•*s*-**phe^{OEt}**]$^+$ and [*s*-**1^D**•H•*r*-**phe^{OEt}**]$^+$complexes, whose *eq*−*eq* forms are 2.0 kcal mol^{-1} less stable than the relevant *ax*−*ax* structures. For both [*r*-**1**•H•*s*/*r*-**naph^{OEt}**]$^+$ diastereomers, the *ax*−*ax* form is more stable than the *eq*−*eq* congener by 1.1 kcal mol^{-1}, in the case of the homochiral complex, and by 0.8 kcal mol^{-1}, in the case of the heterochiral one. The same stability order is calculated for the heterochiral [*r*-**3**•H•*s*-**naph^{OEt}**]$^+$ complex ($\Delta\Delta H°_{(fast-slow)}$ = 1.5 kcal mol^{-1}), while the *eq*−*eq* and *ax*−*ax* structures of its homochiral congener are almost degenerate (Table 3).

The relative abundances, estimated for the more- and less-stable couple of isomers of each complex, are compared in Table 3 with those derived from the experimental kinetic curves. At first glance, the agreement between the two sets of data may appear only partial and qualitative. However, a deeper inspection of Table 3 may remove most of the apparent discrepancies among the reported figures. The occurrence of two stable isomeric forms for the homochiral [*r*-**1**•H•*r*-**phe^{OEt}**]$^+$ (and [*s*-**1^D**•H•*s*-**phe^{OEt}**]$^+$) complex accounts for its biexponential decay with B. On the grounds of their relative stability, the most stable *eq*−*eq* structure is associated with the less reactive [*r*-**1**•H•*r*-**phe^{OEt}**]$^+_{slow}$ (and [*s*-**1^D**•H•*s*-**phe^{OEt}**]$^+_{slow}$) complex and the less stable *ax*−*ax* structure to the more reactive [*r*-**1**•H•*r*-**phe^{OEt}**]$^+_{fast}$ (and [*s*-**1^D**•H•*s*-**phe^{OEt}**]$^+_{fast}$) one. In contrast, the pronounced stability gap (2.0 kcal mol^{-1}) between the *ax*−*ax* and *eq*−*eq* forms of the heterochiral [*r*-**1**•H•*s*-**phe^{OEt}**]$^+$ (and [*s*-**1^D**•H•*r*-**phe^{OEt}**]$^+$) complex justifies the large predominance of a single stable *ax*−*ax* isomer, which is responsible of the observed monoexponential decay with B. An analogous rationale can be advanced for the biexponential decay registered for the diastereomeric [*r*/*s*-**1**•H•*s*-**naph^{OEt}**]$^+$ complexes. Indeed, both diastereomeric complexes show a stable *ax*−*ax* structure, associated with the less reactive [*r*/*s*-**1**•H•*s*-**naph^{OEt}**]$^+_{slow}$ complexes, accompanied by a less stable *eq*−*eq* form, associated with the more reactive [*r*/*s*-**1**•H•*s*-**naph^{OEt}**]$^+_{fast}$ isomers. The same stability order is observed with the heterochiral [*r*-**3**•H•*s*-**naph^{OEt}**]$^+$ complex, whereas the *ax*−*ax* and *eq*−*eq* forms of the homochiral [*s*-**3**•H•*s*-**naph^{OEt}**]$^+$ one are almost degenerate. At variance with the heterochiral [*r*-**1**•H•*s*-**phe^{OEt}**]$^+$ and [*s*-**1^D**•H•*r*-**phe^{OEt}**]$^+$ complexes, the apparent monoexponential decay of the diastereomeric [*r*-**1**•H•*r*/*s*-**phe^{NH}2**]$^+$ pair when reacting with B is not ascribed to the large predominance of a single isomer, but rather to the limited stability difference between their *ax*−*ax* and *eq*−*eq* forms (0.4÷0.6 kcal mol^{-1}; Table 3). If the reactivity of the diastereomeric [*r*-**1**•H•*r*/*s*-**phe^{NH}2**]$^+$ pair toward B is mainly determined by their thermodynamic stability (*vide infra*), their *ax*−*ax* and *eq*−*eq* isomeric forms should display similar reaction 1 rate constants and, therefore, exhibit an apparent monoexponential decay. The same conclusion would be reached for the almost degenerate *ax*−*ax* and *eq*−*eq* forms of the homochiral [*s*-**3**•H•*s*-**naph^{OEt}**]$^+$ complex, if their reactivity toward B were mainly determined by their thermodynamic stability. However, the observation of a biexponential kinetics for the reaction of the homochiral [*s*-**3**•H•*s*-**naph^{OEt}**]$^+$ complex

(23) Bagno, A. *J. Phys. Org. Chem.* **2000**, *13*, 574.
(24) (a) Alcaro, S.; Gasparrini, F.; Incani, O.; Mecucci, S.; Misiti, D.; Pierini, M. and Villani, C. *J. Comput. Chem.* **2000**, *21*, 515. (b) Alcaro, S.; Gasparrini, F.; Incani, O.; Caglioti, L.; Pierini, M.; Villani, C. *J. Comput. Chem.* **2007**, *28*, 1119.;

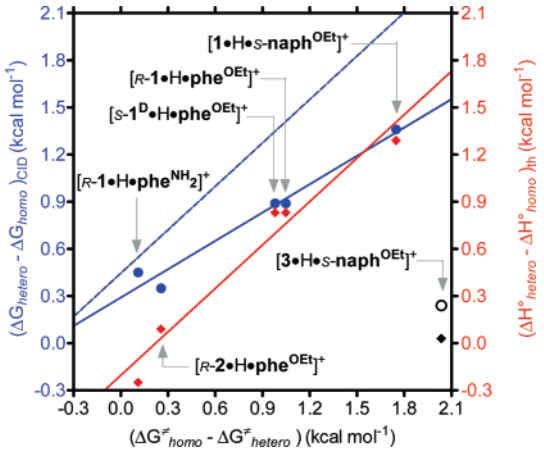

Figure 4. Full red line describes the relationship between the experimental activation barriers of the slow reaction of several two-body $[M•H•A]^+$ complexes with amine B (obtained from the relevant ρ values from Table 1; $\Delta\Delta G^{\#} = \Delta G^{\#}_{homo} - \Delta G^{\#}_{hetero} = -RT \ln \rho$) and the MM computed relative enthalpies of the same $[M•H•A]^+$ complexes ($\Delta\Delta H^{\circ}_{th} = (\Delta H^{\circ}_{hetero} - \Delta H^{\circ}_{homo})_{th}$). The full blue line describes the relationship between the experimental $\Delta\Delta G^{\#} = \Delta G^{\#}_{homo} - \Delta G^{\#}_{hetero} = -RT \ln \rho$ values and the relative stability of the same $[M•H•A]^+$ complexes, calculated at $T_{eff} =$ 298 K from the R values of Table 1 ($\Delta\Delta G_{CID} = (\Delta G_{hetero} - \Delta G_{homo})_{CID} = RT_{eff} \ln R$). If the effective temperature T_{eff} is taken equal to 457 K (broken blue line), both the slopes of the $\Delta\Delta G^{\#}$ vs $\Delta\Delta H^{\circ}_{th}$ and the $\Delta\Delta G^{\#}$ vs $\Delta\Delta G_{CID}$ straight lines coincide and are close to unit (slope = 0.921). This means, by one side, that MM computations correctly estimate the relative stability of the selected $[M•H•A]^+$ complexes and, by the other side, that the stability gap of the diastereomeric $[M•H•A]^+$ reactants (except $[\mathbf{3}•H•s\text{-}\mathbf{naph}^{\mathbf{OEt}}]^+$) is mainly responsible of the enantioselectivity ρ factors of Table 1. All the points refer to reactions with B_R, except that of $[s\text{-}\mathbf{1}^{\mathbf{D}}•H•\mathbf{phe}^{\mathbf{OEt}}]^+$ with B_S.

with B strongly suggests that this hypothesis might be not acceptable in this case (*vide infra*).

The experimental and calculated enantioselectivity factors for hosts **1**−**3**, listed in Table 4, are graphically summarized in Figure 4. A reasonable linear correlation (red line in Figure 4; $r^2 = 0.961$; slope = 0.921; y-intercept = −0.205) does exist between the $\Delta\Delta H^{\circ}_{th} = (\Delta H^{\circ}_{hetero} - \Delta H^{\circ}_{homo})_{th}$ and $\Delta\Delta G^{\#} = \Delta G^{\#}_{homo} - \Delta G^{\#}_{hetero}$ for all the $[M•H•A]^+$ adducts investigated, except $[r/s\text{-}\mathbf{3}•H•s\text{-}\mathbf{naph}^{\mathbf{OEt}}]^+$. The linear relationship suggests that the kinetic enantioselectivity, measured in the FT-ICR experiments at 298 K, is essentially an expression of the stability gap between the corresponding diastereomeric $[M•H•A]^+$ reactants. This conclusion is further supported by the linear correlation between $\Delta\Delta G_{CID} = (\Delta G_{hetero} - \Delta G_{homo})_{CID} = RT_{eff} \ln R$ (taken a $T_{eff} = 298$ K) and $\Delta\Delta G^{\#} = \Delta G^{\#}_{homo} - \Delta G^{\#}_{hetero}$ (blue solid line in Figure 4; $r^2 = 0.971$; slope = 0.601; y-intercept = +0.290). Indeed, if T_{eff} is taken as equal to 457 K, the $\Delta\Delta G^{\#}$ vs $\Delta\Delta G_{CID}$ linear correlation becomes parallel to that of the $\Delta\Delta G^{\#}$ vs $\Delta\Delta H_{th}$ one, though shifted upside by ca. 0.65 kcal mol^{-1} (blue broken line in Figure 4). The pronounced deviation of the $[r/s\text{-}\mathbf{3}•H•s\text{-}\mathbf{naph}^{\mathbf{OEt}}]^+$ systems from the relationships of Figure 4 implies that the enantioselectivity, measured in the FT-ICR experiments at 298K, reflects not only their stability difference, but also the effects of the decamethylene chain of the *r*-**3** host on the relative stability of the diastereomeric transition structures of eq 1. This conclusion is consistent with the observation of a biexponential kinetics for the reaction of B with the homochiral $[s\text{-}\mathbf{3}•H•s\text{-}\mathbf{naph}^{\mathbf{OEt}}]^+$ complex, despite the degeneracy of the *ax*−*ax* and *eq*−*eq* forms of the homochiral $[s\text{-}\mathbf{3}•H•s\text{-}\mathbf{naph}^{\mathbf{OEt}}]^+$ complex. It is concluded that the ρ factors, arising from the FT-ICR experiments with the diastereomeric $[r/s\text{-}\mathbf{3}•H•s\text{-}\mathbf{naph}^{\mathbf{OEt}}]^+$ complexes (Table 2), express the kinetic enantioselectivity of these systems in the guest exchange reaction with B since essentially reflecting the stability difference of the relevant diastereomeric transition structures.

Approach of the Amine B to the $[M•H•A]^+$ Complexes. As already mentioned, analysis of the ρ and ξ factors arising from the kinetic experiments involving the proton-bound complexes between the structurally related hosts M = **1** and **3** and the guest *s*-$\mathbf{naph}^{\mathbf{OEt}}$ indicates that the decamethylene chain in **3** does not influence appreciably the efficiency of the A-to-B displacement, except with the homochiral $[s\text{-}M•H•s\text{-}\mathbf{naph}^{\mathbf{OEt}}]^+_{fast}$ isomer. This latter exception provides a further evidence of the thermodynamic vs kinetic factors controlling the reactivity of the homochiral $[s\text{-}\mathbf{1}•H•s\text{-}\mathbf{naph}^{\mathbf{OEt}}]^+$ and $[s\text{-}\mathbf{3}•H•s\text{-}\mathbf{naph}^{\mathbf{OEt}}]^+$ complexes, respectively, whereas the reactivity of the heterochiral $[r\text{-}\mathbf{1}•H•s\text{-}\mathbf{naph}^{\mathbf{OEt}}]^+$ and $[r\text{-}\mathbf{3}•H•s\text{-}\mathbf{naph}^{\mathbf{OEt}}]^+$ complexes are invariably governed by thermodynamic factors. According to conformational analysis, both hosts **1** and **3** in their *eq*−*eq* and *ax*−*ax* conformations, are characterized by a *saddle roof* shape that differentiates the two sides of the macrocycle. Docking simulations show that all the guests add to the host on the convex surface. Note that, for **3**, this is the only possible approach because the decamethylene chain hinders the approach from the concave side.

In principle, the B amine may approach either the concave or the convex sides of the $[\mathbf{1}•H•A]^+$ complexes to give the most stable $[\mathbf{1}•H•B]^+$ product with B located on the convex side of the host. In the first case, the host must undergo a macrocycle inversion to put B on the new convex side and release A (a *backside* displacement). In the second case, B approaches the complex from the same side where A is located (a *frontside* displacement), and therefore, the release of the guest A does occur without any significant conformational changes of the host. Clearly, the presence of the decamethylene chain in **3** prevents any *backside* displacement in favor of the *frontside* one. That the same frontside approach takes place also with the other $[M•H•A]^+$ structures is suggested by performing a dedicated docking experiment. The global minimum structure of the $[r\text{-}\mathbf{1}•H•r\text{-}\mathbf{phe}^{\mathbf{OEt}}]^+$ complex has been employed in a docking experiment with amine B_R, to form the protonated trimer $[r\text{-}\mathbf{1}•H•r\text{-}\mathbf{phe}^{\mathbf{OEt}}•B_R]^+$. The results confirm that the approach of B_R is energetically more favorable on the convex side by about 3 kcal mol^{-1}. Here, the B_R places its amine group just above the couple of converging C═O fragments on the F2 surface of the host, in a favorable disposition to realize the guest exchange after receiving a proton from the facing NH_3^+ group of the protonated aminoacid (Figure 5).

In this frame, the largely different efficiency observed in the exchange reaction 1 on the homochiral $[M•s\text{-}\mathbf{naph}^{\mathbf{OEt}}]_{fast}$ (M = *s*-**1** (eff = 0.01) and *s*-**3** (eff = 0.20)) isomers can be attributed to the effects of the decamethylene chain in the open *eq*−*eq* conformation of *s*-**3** which may favor the disruption of intramolecular H-bond interactions between the alternate converging CO and NH functionalities placed on the convex F2 face of the host in favor of intermolecular interactions with the B amine approaching the same face.

The Chiral Recognition Model. The formation of the selected $[M•H•A]^+$ complexes is mainly driven by the establishment of a pattern of three strong H-bonds between the protonated amino group of the guest A and the couple of

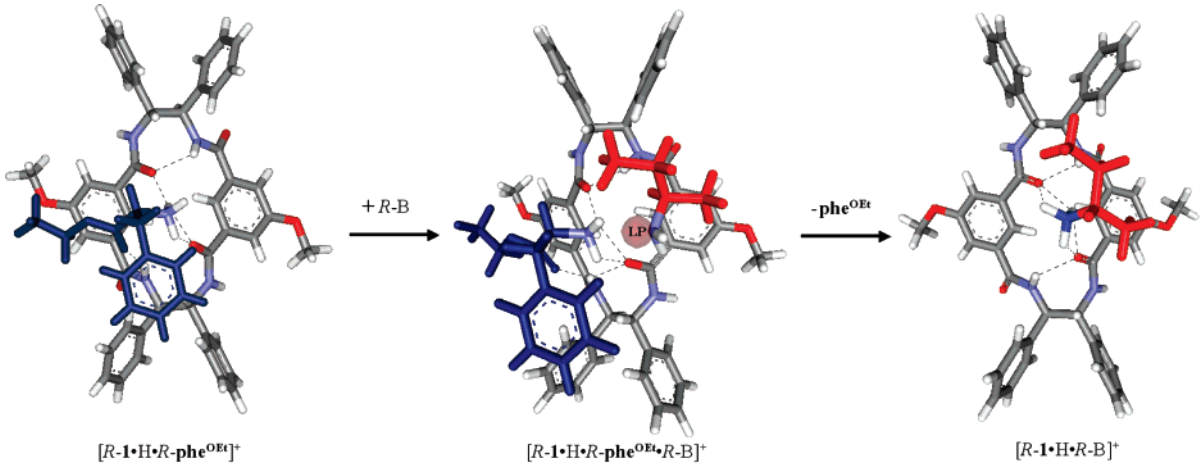

Figure 5. Simulation by docking experiments of the *r*-**phe**$^{\mathbf{OEt}}$ displacement from the [*r*-**1**•H•*r*-**phe**$^{\mathbf{OEt}}$]$^+$ complex by B_R. The most stable structure of the protonated trimer [*r*-**1**•H•*r*-**phe**$^{\mathbf{OEt}}$•B_R]$^+$, obtained by docking procedure, is depicted in the center (LP is the lone-pair of B_R).

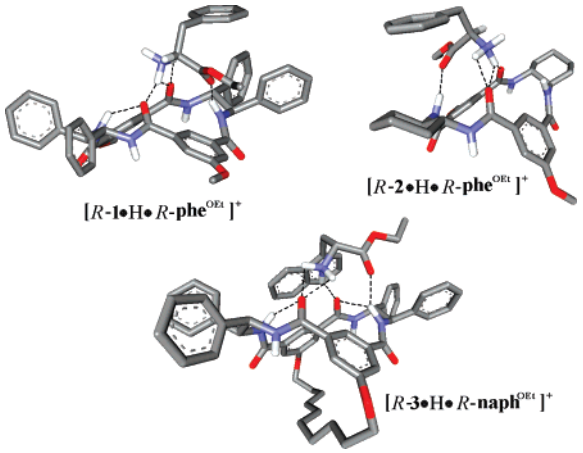

Figure 6. Structures of global minima of the [M•H•*r*-**phe**$^{\mathbf{OEt}}$]$^+$ and [M•H•*r*-**naph**$^{\mathbf{OEt}}$]$^+$ complexes having the host in *eq*−*eq* conformation showing the additional H-bond between the carbonyl oxygen of the guest and one amide N−H of the host.

converging C═O functionalities placed on the F2 surface of the host M. The guest is placed above the center of the host convex side and establishes further weaker interactions with the peripheral zones of the host. In the *eq*−*eq* structures, an additional H-bond is observed between the carbonyl oxygen of the guest and one amide N−H of the host (Figure 6). In the *ax*−*ax* structures with aromatic guests, additional attractive edge-to-face and face-to-face interactions operate between the aromatic moiety of the guest and one isophthalic ring of the host (Figure 7). The extent to which the side-chain groups of the guest either favor or hinder complexation with a given host, depends on the stereochemistry of the guest, and on the size and structure of the side chain itself. This is evident if we consider the very different discrimination ability of host **1** toward the enantiomers of **phe**$^{\mathbf{OEt}}$ and **naph**$^{\mathbf{OEt}}$. We inspected eight geometries of the minimum-energy complexes [*R*-**1**•H•*R/S*-**phe**$^{\mathbf{OEt}}$]$^+$ and [*r*-**1**•H•*r/s*-**naph**$^{\mathbf{OEt}}$]$^+$ obtained by docking experiments. Four of these are the more stable ones having the host in *ax*−*ax* conformation (Figure 8a) and the other four are the more stable with the host in *eq*−*eq* conformation (Figure 8b). Figure 8a clearly shows that all the guests interact with host **1** in *ax*−*ax* conformation in a similar way, placing their aromatic moiety in a face-to-face arrangement above one of the isophthalic rings of the host. The magnitude of these interactions depends on the nature and the configuration of the guest and is somewhat tempered by repulsive interactions, as demonstrated by the significant increase of the distance between the centroids of the opposite phenyl rings of the host when the **phe**$^{\mathbf{OEt}}$ guests (8.80 Å with *r*-**phe**$^{\mathbf{OEt}}$ and 8.97 Å with *s*-**phe**$^{\mathbf{OEt}}$) are replaced by the larger **naph**$^{\mathbf{OEt}}$ ones (9.50 Å with *r*-**naph**$^{\mathbf{OEt}}$ and 9.45 Å with *s*-**naph**$^{\mathbf{OEt}}$). This may account in part for the significant MM-calculated stability difference between the [*r*-**1**•H•*r*-**naph**$^{\mathbf{OEt}}$]$^+$ and [*r*-**1**•H•*s*-**naph**$^{\mathbf{OEt}}$]$^+$ *ax*−*ax* structures ($E_R - E_S = -1.02$ kcal mol^{-1}, Figure 8a), which significantly reduces and even inverts between the [*r*-**1**•H•*r*-**phe**$^{\mathbf{OEt}}$]$^+$ and [*r*-**1**•H•*s*-**phe**$^{\mathbf{OEt}}$]$^+$ ones ($E_R - E_S = 0.34$ kcal mol^{-1}, Figure 8a). Figure 8b reveals that, also with the host in *eq*−*eq* conformation, the enantiomers of **naph**$^{\mathbf{OEt}}$ place their aromatic ring above one isophthalic ring of the host with stabilizing face-to-face (*r*-enantiomer) or edge-to-face (*s*-enantiomer) orientations ($E_R - E_S = -1.32$ kcal mol^{-1}, Figure 8b). In contrast, the most stable *eq*−*eq* [*r*-**1**•H•*r*-**phe**$^{\mathbf{OEt}}$]$^+$ structure shows the phenyl ring of the *r*-**phe**$^{\mathbf{OEt}}$ guest placed just above two adjacent equatorial phenyl rings of the host, thus in a position suitable for intense edge-to-face attractive interactions. Similar interactions are much weaker in the *eq*−*eq* [*r*-**1**•H•*s*-**phe**$^{\mathbf{OEt}}$]$^+$ structure because of the removed position of the guest aromatic ring ($E_R - E_S = -2.00$ kcal mol^{-1}, Figure 8b). Edge-to-face attractive interactions are weak in the most stable *ax*−*ax* [*r*-**1**•H•*s*-**phe**$^{\mathbf{OEt}}$]$^+$ structure as well. This accounts for the stability difference

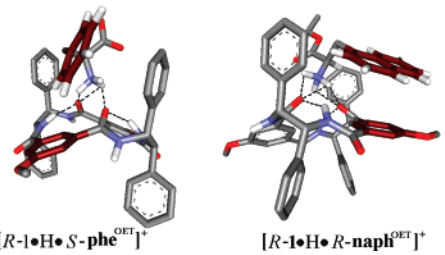

Figure 7. Structures of global minima of the *ax*−*ax* [r-**1**•H•*s*-**phe**$^{\mathbf{OEt}}$]$^+$ and [r-**1**•H•*r*-**naph**$^{\mathbf{OEt}}$]$^+$ complexes showing additional attractive edge-to-face and face-to-face interactions between the aromatic moiety of the guest and one isophthalic ring of the host.

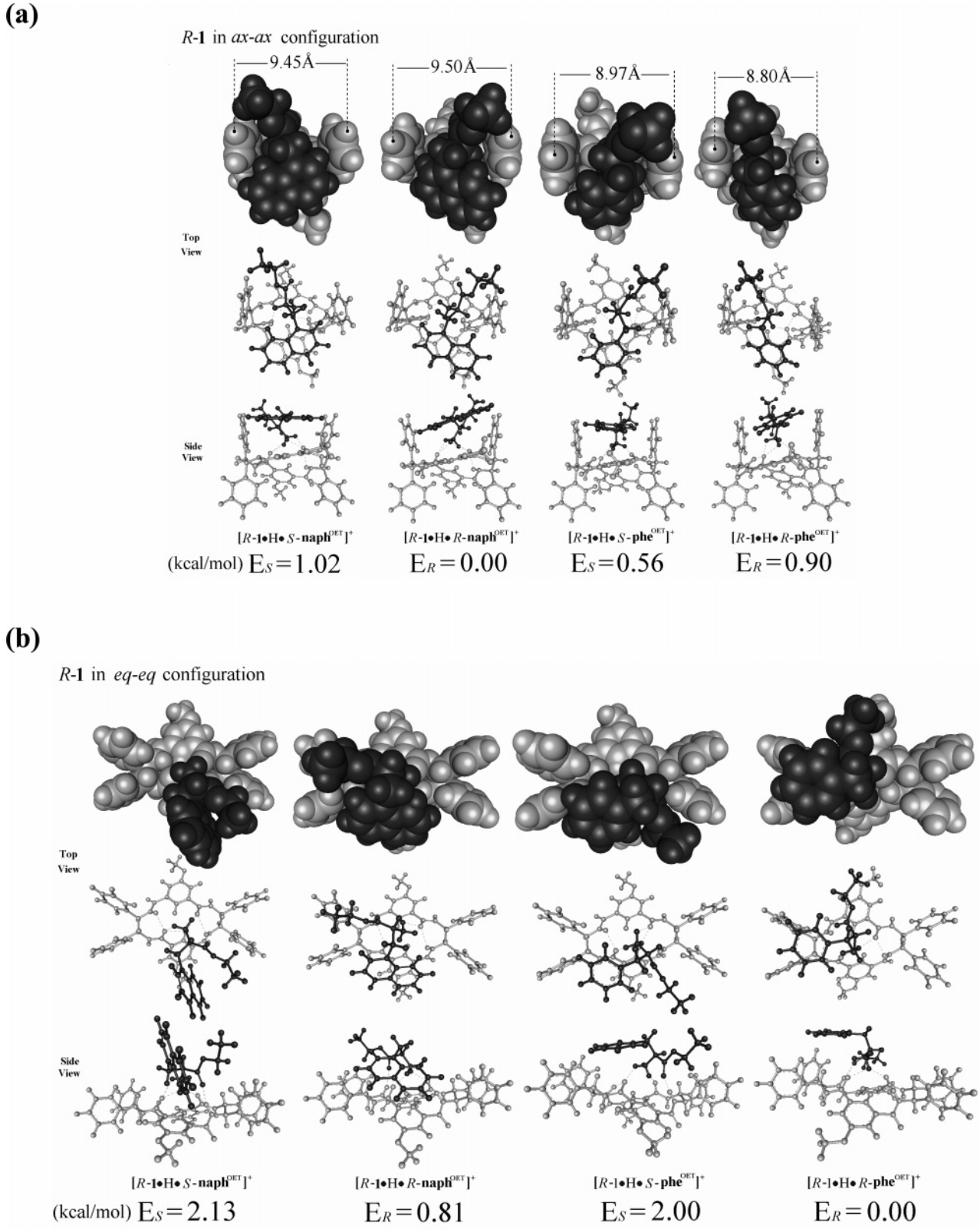

Figure 8. Structure and relative stability of the calculated most stable [*r*-**1**•H•**phe**$^{\mathbf{OEt}}$]$^+$ and [*r*-**1**•H•**naph**$^{\mathbf{OEt}}$]$^+$ diastereomeric complexes having the host either in the *ax*−*ax* (a) or in the *eq*−*eq* (b) conformation employed to analyze the different selectivity showed by host **1** toward the enantiomers of **phe**$^{\mathbf{OEt}}$ and **naph**$^{\mathbf{OEt}}$.

between the most stable *eq*−*eq* and *ax*−*ax* [*r*-**1**•H•**phe**$^{\mathbf{OEt}}$]$^+$ structures ($E_R^{eq-eq} - E_S^{ax-ax} = -0.56$ kcal mol^{-1}, Figure 8a,b).

The aptitude of the **1** and **3** hosts to assume the *ax*−*ax* conformation by complexation enhances their enantiodiscrimination abilities compared to *eq*−*eq*-locked host **2**. The reduced stability gap between the diastereomeric complexes with **3** does not seem to play any appreciable role on the large kinetic enantioselectivity, measured for the same complexes in reaction

1, because the presence of the decamethylene chain probably influence dramatically the relative stability of the corresponding transition structures.

Conclusions

The present MS and computational study provides compelling evidence that the most stable conformers of the selected chiral tetra-amide macrocycles M = **1**−**3** may acquire in the gas phase a different conformation by induced fit on complexation with some representative amino acid derivatives A. This leads to the coexistence in the gas phase of stable diastereomeric $[M•H•A]^+$ *eq*−*eq* and *ax*−*ax* structures, in proportions depending on the configuration of A and M and characterized by different stability and reactivity toward the 2-aminobutane enantiomers.

The gas-phase reaction of the diastereomeric $[M•H•A]^+$ complexes with the enantiomers of 2-aminobutane B obeys either a monoexponential or a biexponential kinetics, depending upon the number and the reactivity of coexisting *eq*−*eq* and *ax*−*ax* structures. The monoexponential kinetics indicate the occurrence of a single $[M•H•A]^+$ structure (as with the heterochiral $[r$-**1**•H•s-**phe**$^{OEt}]^+$ and $[s$-**1**^{D}•H•r-**phe**$^{OEt}]^+$ complexes) or, alternatively, of several stable $[M•H•A]^+$ regioisomers with comparable reactivity (as with the diastereomeric $[r$-**1**•H•r-**phe**$^{NH2}]^+$ pair). In contrast, the biexponential kinetics, observed with the other complexes investigated, are ascribed to the coexistence of two stable $[M•H•A]^+$ isomeric forms with largely different reactivity toward B.

The gas-phase reaction 1 between the selected diastereomeric $[M•H•A]^+$ complexes and the B enantiomers exhibits an enantioselectivity which strongly depends on the structure and the configuration of A and M, but not on that of B. It is verified that the measured kinetic enantioselectivity essentially reflects the free energy gap between the homo- and heterochiral $[M•H•A]^+$ complexes, except when the tetra-amidic host presents the intramolecular decamethylene chain. In this case, the measured enantioselectivity mostly reflects the stability difference between the eq 1 diastereomeric transition structures.

Experimental Section

Mass Spectrometric Experiments. Mass spectra were obtained on a LCQ-Deca XP Plus ion-trap mass spectrometer fitted with an electrospray ionization (ESI) source and a syringe pump. Operating conditions of the ESI source are as follows: spray voltage = + 5.0 kV; sheath gas = 15 AU (Arbitrary Units); capillary voltage = + 27 V; capillary temperature = 210 °C; tube lens offset = 50 V. Methanolic solutions are infused via a syringe pump at a flow rate of 3 μL/min. ESI of solutions of the macrocyclic tetra-amides M = *r*-**1**, *r*-**2**, and *r*-**3** (1×10^{-5} M), containing an equimolar amount of the appropriate amino acid derivative A (Chart 1), leads to the formation of appreciable amounts of the corresponding $[M•H•A]^+$ and $[(M)_2•H•A]^+$ complexes. After individual isolation by broad-band ejection of the accompanying ions, the isolated ions are then subjected to a supplementary ac signal to resonantly excite them and cause fragmentation by collisions with He gas (CID). Ion excitation time for CID is 30 ms with the amplitude of the excitation AC kept the same for the measurements of two enantiomeric guests with the same host. Optimized instrumental values of relative collision energy of 12−15% give exclusively the fragment ions of interest (relative collision energy values range 0−100% corresponding to 0−5 V resonant excitation potential). Spectra acquired in the centroid mode are the average of about 100 scans, each consisting of three averaged microscans.

Kinetic experiments were performed at room temperature in an APEX 47e FT-ICR mass spectrometer equipped with an ESI source (Bruker Spectrospin) and a resonance cell ("infinity cell") situated between the poles of a superconducting magnet (4.7 T). Stock solutions of the macrocyclic tetra-amides M = *r*-**1**, *s*-**1**^{D}, *r*-**2**, *r*-**3**, and *s*-**3** (1×10^{-5} M) in CH_3OH, containing an equimolar amount of the appropriate amino acid derivative A (*A* = *r*/*s*-**phe**, *r*/*s*-**phe**^{OEt}, and *s*-**naph**^{OEt}), were electrosprayed through a heated capillary (130 °C) into the external source of the FT-ICR mass spectrometer. The resulting ions were transferred into the resonance cell by a system of potentials and lenses and quenched by collisions with methane pulsed into the cell through a magnetic valve. Abundant signals, corresponding to the natural isotopomers of the proton-bound complex $[M•H•A]^+$, were monitored and isolated by broad-band ejection of the accompanying ions. The $[M•H•A]^+$ family was then allowed to react with the chiral amine B present in the cell at a fixed pressure whose value ranges from 6.0×10^{-8} to 2.9×10^{-7} mbar depending upon its reactivity. Accurate measurement of the B pressure in the resonance cell necessitates the use of an ion gauge whose sensitivity is dependent on the nature of the chemical species. The correction of the ionization gauge reading is achieved by first determining the rate constant of the reaction between the CH_4^+ radical cation and CH_4 in the FT-ICR instrument at a given nominal methane pressure and then by comparing the obtained result with the average value of reported rate constants for this process (1.13×10^{-9} cm^3 molecule^{-1} s^{-1}).[25] Subsequently, the correction factor needed for amine B may be estimated with the method based on an indicated linear dependence of the response of the ionization gauge with the polarizability of the base in question.[26]

Computational Details. Molecular mechanics calculations and docking simulations *in vacuo* of the bimolecular adducts between the chiral macrocycles *r*-**1,** *r*-**2** and *r*-**3** and the protonated aminoacidic derivatives **phe**^{OEt}, **phe**^{NH2}, and **naph**^{OEt}, as well as between the $[r$-**1**•H•r-**phe**$^{OEt}]^+$ complex and the *r*-2-aminobutane B_R, were achieved in three steps:

(i) conformational search of host and guest molecules was carried out by Batchmin and Macromodel version 4.5 (Columbia University, NY) using the following options: MM2* Force Field, Montecarlo stochastic algorithm with 3000 generated structures, minimization by PR conjugate gradient. All the rotatable bonds were explored. The obtained geometries were analyzed by the home made computer program C.A.T.[24] to exclude twin molecules and to make clusters based on energetic and geometric criteria;

(ii) rigid docking was performed on each couple of host and guest molecules using the MolInE program. The host−guest approach options set were: 52 directions of translation and 272 relative orientations of guest to host for each couple of host−guest conformations;

(iii) the ensemble of adducts obtained in the second step was submitted to selection by using either energetic and geometric criteria. The geometry of the so achieved complexes was optimized by full relaxing their structure using the Batchmin program with the following options set: MM2* Force Field, PR conjugate gradient minimization. All the conformer ensembles were analyzed by C.A.T. program to exclude twin molecules, make energetic clusters and perform calculations of both Boltzmann populations and thermodynamic quantities related to the simulated complexes.

Ab initio DFT calculations on the $[r$-**1**•H•r-**phe**$^{OEt}]^+$ and $[r$-**1**•H•s-**phe**$^{OEt}]^+$ complexes were carried out using the Gaussian 03 suite of programs[27] installed on dual processor Opteron workstations. The calculations were carried out at the B3LYP/6-31G*[28] level of theory. At the same level of theory, frequency calculations were performed for all the optimized structures to ascertain their minimum or transition

(25) Ikezoe, Y., Matsuoka, S., Takebe, M., Viggiano, A. A. *Gas-Phase Ion − Molecule Reaction Rate Constant through 1986*; Maruzen Company, Ltd.: Tokyo, 1987.
(26) Bartmess, J. E.; Georgiadis, R. M. *Vacuum* **1983**, *33*, 149.
(27) (a) Becke, A. D. *J. Chem. Phys*. **1993**, *98*, 1372, 5648. (b) Lee, C.; Yang, W.; Parr, R. G. *Phys. Rev. B* **1988**, *37*, 785.
(28) Frisch, M. J.; et al. *Gaussian 03*, revision C.02; Gaussian,Inc.: Wallingford, CT, 2004.

state nature. The *ax*−*ax* and *eq*−*eq* conformers of [*r*-**1**•H•*r*-**phe**$^{\mathbf{OEt}}$]$^+$ have been reoptimized at the B3LYP/6-311+G** level of theory. No appreciable structural differences have been observed relative to those calculated at the B3LYP/6-31G* level of theory.

Acknowledgment. Work supported by the Ministero dell'Istruzione dell'Università e della Ricerca (MIUR, PRIN contract no. 2005037725) and FIRB contract no. RBPR05NWWC_003) and the Consiglio Nazionale delle Ricerche (CNR). MS and AF express their gratitude to F. Angelelli for technical assistance.

Supporting Information Available: Synthesis of macrocycle **3**. Most stable B3LYP/6-31G*-optimized structures of the *eq*−*eq*, *ax*−*ax*, and *ax*−*eq* conformers of the diastereomeric [*r*-**1**•H•**phe**$^{\mathbf{OEt}}$]$^+$ complexes. Kinetic plots. This material is available free of charge via the Internet at http://pubs.acs.org.

JA073287+